Materials Advances

ROYAL SOCIETY OF CHEMISTRY

PAPER

View Article Online
View Journal | View Issue

Cite this: *Mater. Adv.*, 2024, 5, 3281

Halogen substituted tetraphenylethylene AIEgens: facile single-crystal-to-single-crystal transformation, polymorphism and mechanofluorochromism†

Yong Cao, [a] Chengjun Pan *[ab] and Jinjia Xu *[b]

The molecular structure and supramolecular organization of fluorophores play an important role in generating solid-state fluorescent materials and understanding the mechanism of fluorescence switching/tuning. Molecules that retain the single crystalline nature after applying external stimuli can provide a deep insight into precise control over fluorescence modulation. Herein, we reported the synthesis of eight halogen-substituted tetraphenylethylene (**TPE**) aggregation-induced emissive (AIEgens) derivatives and investigated the impact of the halogens (F, Cl, Br, and I) on polymorphism and topochemical structural transformation. **TPE** derivatives with F showed the highest fluorescence (Φ_f = 58–91%) and heavy atom substitution (I) reduced the fluorescence (Φ_f = 14–16%). Solid-state structural studies revealed the formation of polymorphs in **ClTPE** and **BrTPE** derivatives whereas **FTPE** and **ITPE** did not show any polymorphs. The PXRD and DSC studies were further performed to substantiate polymorph formation, which revealed that the formation of stronger intermolecular interactions in **FTPE** prevented polymorph formation. Importantly, the **ClTPE** polymorph exhibited facile single-crystal-to-single-crystal structural transformation upon heating/solvent exposure. The formation of polymorphs, structural transformation and crystal growth characteristics from different solvents produced tuneable and switchable fluorescence. A twisted non-planar **TPE** unit was also prepared to demonstrate mechanical pressure-induced reversible fluorescence switching. The present work attempted to explore the structural design principles for generating polymorphs and facilitating topochemical transformations in AIEgens, which will enhance our comprehensive understanding of the mechanism underlying fluorescence switching/tuning.

Received 19th January 2024,
Accepted 17th February 2024

DOI: 10.1039/d4ma00059e

rsc.li/materials-advances

Introduction

Organic solid-state fluorescent materials with tunable and switchable fluorescence are considered to be potential materials for various applications including organic light-emitting semiconductors, information storage, sensors and bioimaging.[1–7] The fluorescence efficiency of organic molecules in the solid state is strongly influenced by different factors such as molecular motions, conjugation, molecular structures, functional groups, and intermolecular interactions.[8–11] Particularly, fluorophore structures and supramolecular interactions controlled molecular organization exerting a strong impact on the fluorescence efficacy as well as fluorescence switching and tuning.[10–13] For example, the strong fluorescence of aromatic conjugated rigid molecules was significantly quenched due to the aggregation-caused quenching effect in the solid state.[14] In contrast, aggregation-induced strongly enhanced emission was observed for a class of non-planar organic fluorophores that hindered strong aromatic π–π stacking in the solid state.[15,16] Structure–property mechanistic studies suggested that intermolecular interactions facilitated molecular rigidification and restriction of intramolecular rotation, suppression of Kasha's rule of fluorescence and excimer formation and restricted access to conical intersection could account for aggregation-induced emission (AIE).[17,18] Engineering intermolecular interactions with subtle structural change and polymorphism by using conformationally flexible fluorophores resulted in tunable fluorescence.[19–22] For instance, nitrophenyl substitution with the tetraphenylethylene (**TPE**) core restricted the intersystem crossing process and produced on–off reversible mechanofluorochromic materials.[23] Discrete dimers with weak π–π interactions in benzothiazole molecules exhibited a mechanical pressure-induced remarkable fluorescence

[a] *Shenzhen Key Laboratory of Polymer Science and Technology, College of Materials Science and Engineering, Shenzhen University, Shenzhen 518060, China. E-mail: pancj@szu.edu.cn*
[b] *Department of Chemistry and Biochemistry, University of Missouri, St Louis, MO, 63121, USA. E-mail: jxbgk@umsystem.edu*

† Electronic supplementary information (ESI) available: NMR, MS, absorption, and fluorescence spectra, DSC and PXRD, single crystal structural packing, and fluorescence images. See DOI: https://doi.org/10.1039/d4ma00059e

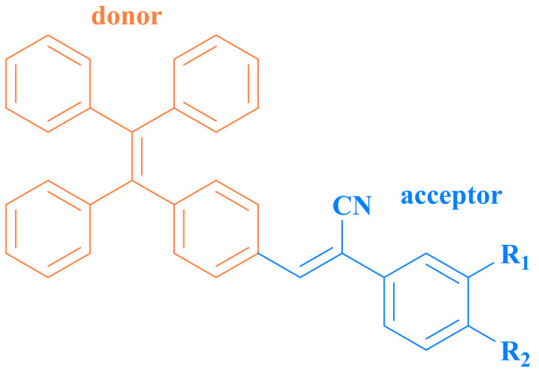

R_1 = F, R_2 = H **(3FTPE)**; R_1 = H, R_2 = F **(4FTPE)**
R_1 = Cl, R_2 = H **(3ClTPE)**; R_1 = H, R_2 = Cl **(4ClTPE)**
R_1 = Br, R_2 = H **(3BrTPE)**; R_1 = H, R_2 = Br **(4BrTPE)**
R_1 = I, R_2 = H **(3ITPE)**; R_1 = H, R_2 = I **(4ITPE)**

Fig. 1 Molecular structure of halogen substituted **TPE** derivatives.

shift and high sensitivity.[24] Switching molecular packing between crystalline and amorphous phases under external stimuli is the most common method attributed to fluorescence control.[25–27] However, the lack of clear molecular organization information about the amorphous phase makes it difficult to elucidate the mechanism of fluorescence modulation. On the other hand, achieving reversible crystal-to-crystal transition at the molecular level by polymorphs is a promising strategy for understanding fluorescence switching mechanisms.[28,29] But weak intermolecular interaction driven organic molecular systems rarely preserve the single crystalline nature and exhibit reversible structural transformation.[30]

Halogen bonding has been widely employed as a supramolecular non-covalent interaction to achieve desired molecular assembly in liquid crystals and electronic and magnetic materials.[31–33] Halogens in organic fluorophores can regulate the intermolecular interaction that might facilitate the improvement of solid state fluorescence.[34–39] Br···Br interaction in highly planar enaminone fluorophores blocked nonradiative pathways efficiently and facilitated radiative processes.[40] Br substitution in phenothiazine-based benzoxazole derivatives disrupted π–π stacking and produced stronger mechanofluorochromism.[41] Halogen substitution in carbazole-based derivatives showed polymorphism and substituent dependent enhancement.[42] Furthermore, heavy halogens such as Br and I can increase spin–orbit coupling *via* heavy atom effects that efficiently quench singlet excited states and promote singlet-to-triplet intersystem crossing and *vice versa*.[43,44] Heavy atom effects and halogen interactions were included to develop interesting phosphorescent materials.[45–47] The insignificant impact of halogen substitution as well as strong quenching by heavy atom substitution on fluorescence has also been reported.[48–50] These varied responses and fluorescence modulation by controlling intermolecular interactions deserve more investigation with halogen-substituted fluorophores to better establish the structure–property relationship. In this study, we have synthesized a series of **TPE**-based donor–acceptor derivatives (Fig. 1) and explored the impact of halogen atoms and substitution positions on the molecular arrangements, single-crystal to single-crystal topochemical structural transformation polymorphism and mechanofluorochromism. Although halogen substitution did not have a significant impact on the fluorescence shift, the fluorescence efficiency was gradually reduced from F to I. DSC and powder XRD (PXRD) studies of Cl and Br substituted compounds further demonstrated the interesting polymorphism and single-crystal to single-crystal structural transformation.

Results and discussion

TPE-halogen donor–acceptor derivatives were synthesized by a condensation reaction between **TPE**-aldehyde and the corresponding halogen-substituted phenylacetonitrile (details in Scheme S1, ESI†). All the molecules exhibited typical

Table 1 Fluorescence emission wavelength (λ_{max}) and absolute quantum yield (Φ_f) of crystals grown in various solvents

Compounds	Solvents for crystallization	Polymorphs	λ_{max} (nm)	Φ_f (%)	Compounds	Solvents for crystallization	Polymorphs	λ_{max} (nm)	Φ_f (%)
3FTPE	CH_3CN	Polymorph-1	490	58	**4FTPE**	CH_3CN	—	—	—
	MeOH		478	66		MeOH	Polymorph-1	493	66
	DMF		483	81		DMF		488	91
	DMSO		487	73		DMSO		491	80
3ClTPE	CH_3CN	Polymorph-1	494	29	**4ClTPE**	CH_3CN	Polymorph-1	491	51
	MeOH		499	25		MeOH	Polymorph-2	503	34
	DMF	—	—	—		DMF		497	41
	DMSO	—	—	—		DMSO		494	43
3BrTPE	CH_3CN	Polymorph-1	497	39	**4BrTPE**	CH_3CN	Polymorph-1	487	47
	MeOH		495	38		MeOH	Polymorph-2	509	33
	DMF	—	—	—		DMF		496	36
	DMSO	Polymorph-2	492	50		DMSO		496	37
3ITPE	CH_3CN	Polymorph-1	492	16	**4ITPE**	CH_3CN	—	—	—
	MeOH		492	16		MeOH	—	—	—
	DMF		503	14		DMF	—	—	—
	DMSO	—	—	—		DMSO	—	—	—

"—" means that the compound had poor crystallinity in the corresponding solvents and no single crystal was obtained.

aggregation-induced emission in the solid state as in previous reports.[28,51,52] Crystallization of halogen-substituted **TPE** derivatives was attempted using different solvents in order to obtain polymorphs for the further topochemical structural transformation study (the procedure for crystal growth is shown in Fig. S1 and S2, ESI†). Table 1 summarizes the crystallization solvent lists, polymorph details, and related fluorescence properties. **TPE** derivatives with halogen atoms showed strongly enhanced solid-state fluorescence. Fluorescence emission wavelength λ_{max} did not vary significantly with the variation of the halogen atom. Fluorine-substituted **FTPE** molecules exhibited the highest fluorescence efficiency of 91% whereas other heavy atoms such as Br and I substitution reduced the fluorescence with a quantum yield of 14–16%. The solvents of crystallization influenced the fluorescence λ_{max} *via* producing polymorphs or due to crystal habits. The fluorescence λ_{max} of these crystals can be visualized with color changes shown in fluorescence images (Fig. S3, ESI†).

Single crystal structural analysis of halogen substituted **TPE** derivatives showed varying intermolecular interactions and molecular packing in the crystal lattice. It is noted that the **TPE** core unit displayed a twisted molecular conformation. However, the **TPE** phenyl donor and phenylacetonitrile acceptor adopted a coplanar/twisted conformation depending on the substitution (Table S1, ESI†). **FTPE** and **ITPE** exhibited a coplanar conformation, while **ClTPE** and **BrTPE** adopted a coplanar/twisted conformation. The extent of twisting was also significantly influenced by the halogen. **3FTPE** crystals grown from different solvents produced the same structure and packing (Fig. S4(a) and (c), ESI†). H-bonding interaction between F and phenyl hydrogen produced a dimer that was further linked by cyano nitrogen H-bonding with phenyl hydrogen (Fig. S4b, ESI†). Furthermore, similar PXRD patterns of **3FTPE** crystals ruled out any polymorphism (Fig. S5a, ESI†). DSC studies of **3FTPE** crystals exhibited only a melting point of 174 °C (Fig. S5b, ESI†). **4FTPE** contained four molecules in the asymmetric unit (Fig. S6a, ESI†). F intermolecular interaction with phenyl hydrogen in the crystal lattice of **4FTPE** produced a helical network structure (Fig. S6b, ESI†). The molecular packing diagram exhibited opposite molecular arrangement. **4FTPE**

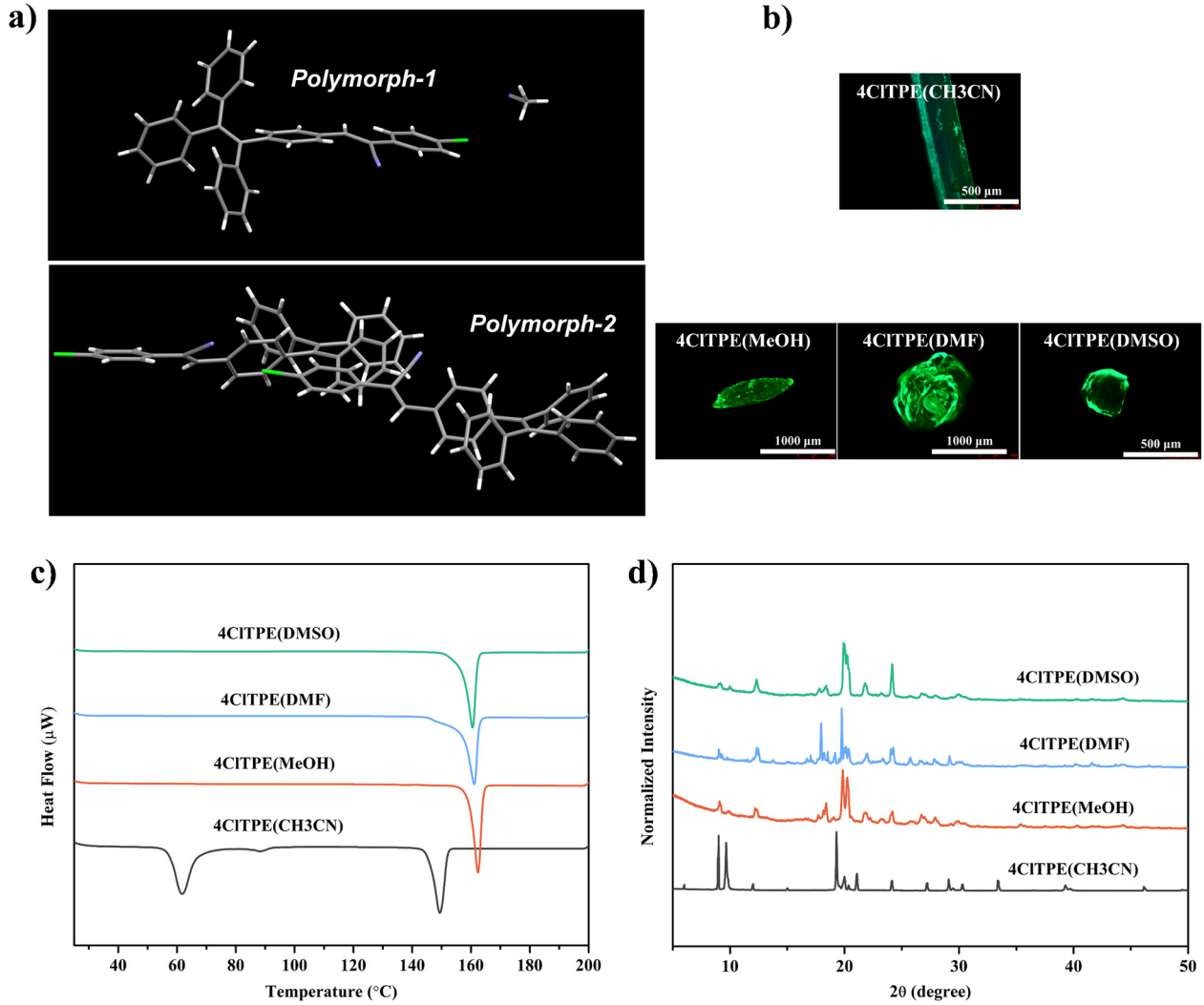

Fig. 2 Molecular conformation (a), fluorescence images (b), DSC analysis (c) and PXRD analysis (d) of 4ClTPE crystals.

crystals grown from different solvents did not show any polymorphism that was further confirmed by PXRD and DSC studies (Fig. S7, ESI†). **3ITPE** also did not produce any polymorphic structures (Fig. S8, ESI†). Intermolecular interactions between I and the carbon on the phenyl group connected the crystal network (Fig. S9b, ESI†). It should be noted that our attempt with **4ITPE** for obtaining quality crystals was not successful.

Although **3ClTPE** crystals did not show any polymorphism (Fig. S10, ESI†), the **TPE** phenyl donor and phenyl acetonitrile acceptor exhibited coplanar and slightly twisted molecular conformations. The asymmetric unit of **3ClTPE** contained two molecules in the crystal lattice (Fig. S11a, ESI†). The weak intermolecular interactions between Cl and phenyl hydrogen resulted in a cyclic structure (Fig. S11b, ESI†). Molecular packing revealed opposite molecular organization (Fig. S11c, ESI†). However, two different crystal structures of **4ClTPE** were obtained. **4ClTPE** crystals obtained from CH_3CN revealed inclusion of solvent molecules in the crystal lattice (Fig. 2a(polymorph-1)). The weak intermolecular interactions between acetonitrile nitrogen and phenylacetonitrile hydrogen stabilize the solvent molecules in the crystal lattice (Fig. S12b, ESI†). The inclusion of acetonitrile hindered close interaction between **4ClTPE** molecules. On the other hand, CH_3OH/DMF/DMSO grown crystals of **4ClTPE** showed polymorphism. The asymmetric unit containing two molecules did not include any solvent molecules (Fig. 2a(polymorph-2)). Cl halogen interaction with cyano nitrogen and C–H$\cdots\pi$ interactions between **TPE** units produced a network structure (Fig. S12d. ESI†). Molecules adopted opposite molecular packing in the solid state (Fig. S12e, ESI†). PXRD of **4ClTPE** crystals also confirmed the formation of polymorphs in CH_3CN and CH_3OH/DMF/DMSO (Fig. 2d). DSC studies of **4ClTPE** crystals grown from acetonitrile showed a clear phase transition at 57 °C before melting at 146 °C (Fig. 2c). However, CH_3OH/DMF/DMSO grown **4ClTPE** crystals melted at 157 °C without any phase transition. Interestingly, bromo-substituted **3BrTPE** and **4BrTPE** produced fluorescent polymorphs. **3BrTPE** crystals grown from DMSO showed inclusion of solvent molecules in the crystal lattice (Fig. S13c, ESI†). But CH_3CN/CH_3OH grown crystals did not show any solvent molecule in the crystal lattice (Fig. S13a, ESI†). The inclusion of DMSO led to higher molecular twisting between the **TPE** phenyl donor and the phenyl acetonitrile acceptor whereas a coplanar conformation was observed in CH_3CN grown crystals. PXRD and DSC studies further supported the formation of polymorphs in **3BrTPE** crystals (Fig. S14, ESI†). The crystals grown from DMSO showed a phase transition at 88 °C before melting at 193 °C. In contrast, CH_3CN/CH_3OH grown crystals melted at 161 °C and did not show any phase transition. Intermolecular interactions between cyano nitrogen and phenylacetonitrile hydrogen produced a network structure in the crystal lattice (Fig. S13b, ESI†). The adjacent molecules adopted opposite molecular orientation in DMSO grown crystals whereas the same side orientation was observed in CH_3CN/CH_3OH grown crystals (Fig. S13(d) and (b), ESI†). However, the next layer in CH_3CN/CH_3OH grown crystals displayed the opposite orientation. Similar to **4ClTPE**, **4BrTPE** crystals grown from CH_3CN included the solvent molecule in the crystal lattice (Fig. S15a, ESI†). Crystals grown from CH_3OH/DMF/DMSO showed the same structure without any

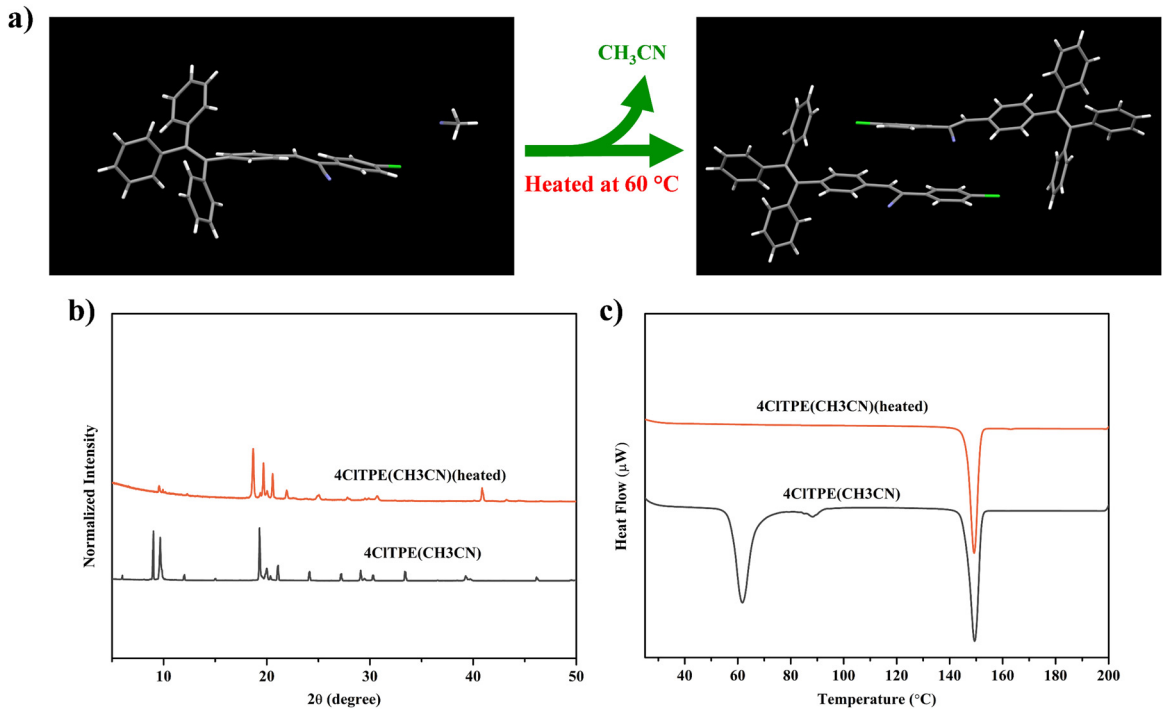

Fig. 3 Single crystal-to-single crystal transition (a), PXRD analysis (b) and DSC analysis (c) of the **4ClTPE** (CH_3CN) crystal under thermal stimulation.

Table 2 Fluorescence emission wavelength (λ_{max}) and absolute quantum yield (Φ_f) of crystals (**4ClTPE**(CH_3CN) and **3BrTPE**(DMSO)) before and after thermal stimulation

Compounds	Crystals	λ_{max} (nm)	Φ_f (%)
4ClTPE	4ClTPE(CH_3CN)	491	51
	4ClTPE(CH_3CN)(heated)	490	45
3BrTPE	3BrTPE(DMSO)	492	50
	3BrTPE(DMSO)(heated)	506	39

solvent molecules (Fig. S15c, ESI†). PXRD also supported the polymorphism by showing different patterns for crystals grown from CH_3CN (Fig. S16a, ESI†). DSC studies showed clear phase transition at 51 °C before melting at 172 °C for crystals grown from CH_3CN (Fig. S16b, ESI†). The other polymorph showed only a melting point of 172 °C. The molecular conformation and packing of **4BrTPE** crystals were also similar to those of **4ClTPE** crystals (Fig. S12 and S15, ESI†). The donor and acceptor units adopted a nearly coplanar conformation in CH_3CN polymorphs whereas a twisted conformation was observed in polymorphs obtained from CH_3OH/DMF/DMSO. Through single crystal structure analysis of these **TPE** derivatives, we found that the interaction of halogen atoms with other molecules plays an important role in the formation of crystals. Under the same crystallization conditions, **TPE** derivatives substituted by F with the smallest atomic radius and the strongest electronegativity exhibited good crystallinity and were conducive to producing crystals of the same structure. However, compounds substituted by I, which has the largest atomic radius and the weakest electronegativity, had poor crystallinity and not even crystals could be obtained. Only **ClTPE** and **BrTPE** tended to produce polymorphs. Crystal habits and polymorphism halogen substituted **TPE** derivatives contributed to fluorescence modulation.

Furthermore, the polymorphic crystals were explored for single-crystal-to-single-crystal structural transformation by heating. **4ClTPE** crystals grown from CH_3CN that included solvent molecules in the crystal lattice lost the solvent molecules upon heating. Interestingly, the crystals retained their single crystalline nature. Single crystal analysis confirmed the removal of solvent molecules (Fig. 3a). Intermolecular

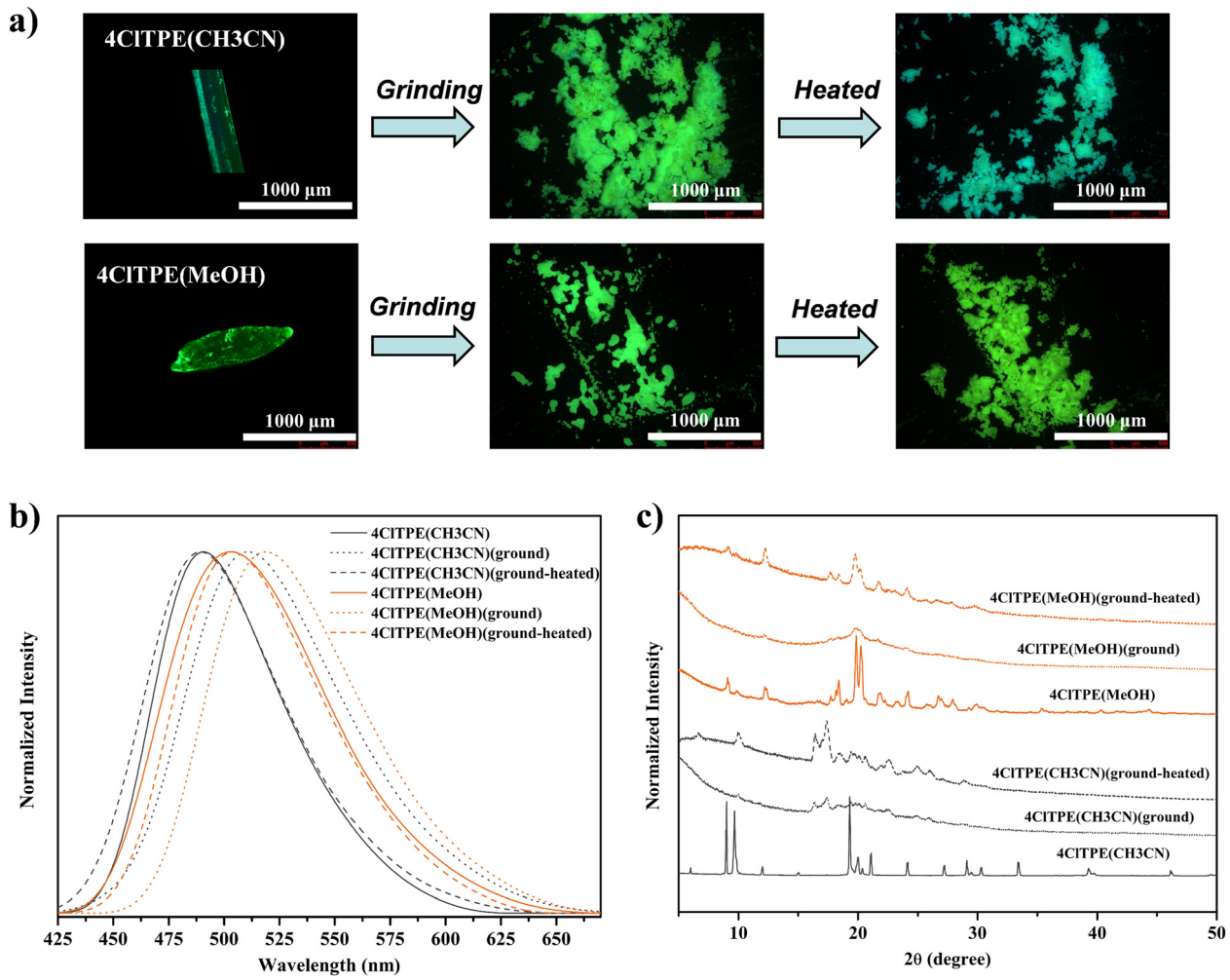

Fig. 4 Mechanofluorochromism of **4ClTPE** crystals in grinding and subsequent heating. Fluorescence images (a), fluorescence emission spectra (λ_{ex} = 370 nm) (b) and PXRD analysis (c).

Table 3 Fluorescence emission wavelength (λ_{max}) and absolute quantum yield (Φ_f) of mechanofluorochromism of **4ClTPE** and **3BrTPE** crystals

Compounds	Crystals	λ_{max} (nm)	Φ_f (%)	Crystals	λ_{max} (nm)	Φ_f (%)
4ClTPE	4ClTPE(CH_3CN)	491	51	4ClTPE(MeOH)	503	34
	4ClTPE(CH_3CN)(ground)	511	40	4ClTPE(MeOH)(ground)	519	46
	4ClTPE(CH_3CN)(ground-heated)	489	52	4ClTPE(MeOH)(ground-heated)	504	27
3BrTPE	3BrTPE(CH_3CN)	497	39	3BrTPE(DMSO)	492	50
	3BrTPE(CH_3CN)(ground)	514	45	3BrTPE(DMSO)(ground)	506	52
	3BrTPE(CH_3CN)(ground-heated)	492	45	3BrTPE(DMSO)(ground-heated)	499	57

interactions between cyano nitrogen and phenylacetonitrile hydrogen connected the supramolecular dimers. After heating, PXRD of the treated sample showed clearly different patterns and the phase transition peak in DSC has also disappeared (Fig. 3(b) and (c)). In contrast, the solid state fluorescence of **4ClTPE** before and after heating did not show any significant variation (Fig. S18(a), (c), ESI† and Table 2) although polarized optical microscopy images exhibited clear differences before and after heating the crystals (Fig. S18b, ESI†). The fluorescence efficiency of the **4ClTPE** solid was slightly reduced after heating (Φ_f = 45% (after heating) and 51% (before heating))(Table 2). Comparing the molecular conformation and packing of the crystals before and after heating (Fig. S12b and S17c, ESI†), it was found that there was no significant change. Just as the acetonitrile molecules disappeared, the face-to-face stacking became tighter. This should be the reason why the fluorescence λ_{max} did not change but the fluorescence efficiency decreased after the crystals were heated.[53] Heating of **3BrTPE** crystals grown from DMSO also produced different PXRD patterns and indicated structural conversion (Fig. S19d, ESI†). DSC of heated **3BrTPE** crystals did not show any phase transition that further supported the structural transformation (Fig. S19c, ESI†). However, the crystals lost their single crystalline character and hence structural studies could not be performed. The solid state fluorescence of **3BrTPE** showed clear modulation before and after heating (Fig. S19(a) and (b), ESI† and Table 2). Before heating, it showed fluorescence at 492 nm that was shifted to 506 nm after heating. Similarly, **4BrTPE** crystals grown from CH_3CN also exhibited structural transformation upon heating. PXRD showed different patterns after heating and the phase transition in **4BrTPE** CH_3CN also disappeared in DSC charts (Fig. S20(d) and (c), ESI†). However, similar to **4ClTPE**, **4BrTPE** crystals grown from CH_3CN did not show any significant fluorescence modulation before and after heating (Fig S20(a) and (b), ESI†). The loss of single crystalline nature hindered single crystal structural studies.

TPE derivatives with a twisted non-planar molecular structure are known to exhibit stimuli-induced reversible fluorescence switching.[54–56] **4ClTPE** and **3BrTPE** crystals were chosen as representative examples for demonstrating mechanical pressure induced reversible fluorescence switching. The fluorescence of **4ClTPE** crystals grown from CH_3CN showed a red shift from 491 to 511 nm upon crushing whereas heating reversed the fluorescence to 489 nm (Fig. 4(a), (b) and Table 3). Similarly, **3BrTPE** crystals grown from CH_3CN showed a fluorescence change from 497 to 514 nm upon crushing and the fluorescence was reversed to 492 nm upon heating (Fig. S22b, ESI† and Table 3). Fluorescence images also showed a clear colour change upon crushing and heating (Fig S22a, ESI†). In general, reversible fluorescence switching was attributed to the transformation of the crystalline phase to the amorphous phase.[57–59] The sharp PXRD peaks for **4ClTPE** and **3BrTPE** indicated the crystalline nature of the compounds (Fig. 4c and Fig. S22c, ESI†). However, the peak intensities were significantly reduced after crushing which suggested conversion of the crystalline to the amorphous/partial amorphous phase. The crystallinity was regained upon heating. Hence PXRD indicated reversible phase transformation from the crystalline to the amorphous phase and *vice versa* that contributed to reversible fluorescence switching.

Conclusions

In summary, eight halogen-substituted **TPE** derivatives were synthesized and demonstrated halogen-dependent polymorphism, topochemical conversion, and solid-state fluorescence. Halogen substitution did not alter the fluorescence emission wavelength significantly. But the fluorescence efficiency was strongly influenced by halogen. **FTPE** exhibited highly enhanced solid-state fluorescence compared to **ITPE** compounds. **ClTPE** and **BrTPE** derivatives produced polymorphism depending on the solvents of crystallization. The formation of polymorphs was further confirmed by PXRD and DSC studies. Interestingly, polymorphs including solvent molecules exhibited topochemical conversion upon heating the crystals and retained their single crystalline nature. Single crystal structural studies, PXRD, and DSC analysis indicated the formation of a new polymorphic structure. Halogen-substituted **TPE** derivatives showed reversible mechanofluorochromism upon crushing and heating. PXRD studies indicated that reversible phase transformation between crystalline and amorphous contributed to reversible fluorescence switching. The present work attempted to explore the structural design principles for generating polymorphs and facilitating topochemical transformations in AIEgens will enhance the comprehensive understanding of the mechanism underlying fluorescence switching/tuning.

Conflicts of interest

There are no conflicts to declare.

Acknowledgements

The authors would like to thank the support from the Banavali Green and Sustainable Chemistry Fund in Arts and Science at the University of Missouri – St Louis, USA. Dr Savarimuthu Philip Anthony from SASTRA Deemed University, India, is greatly acknowledged for his contribution at the initial stage of this work.

Notes and references

1 M. Y. Wong and E. Zysman-Colman, *Adv. Mater.*, 2017, **29**, 1605444.
2 J. M. Ha, S. H. Hur, A. Pathak, J.-E. Jeong and H. Y. Woo, *NPG Asia Mater.*, 2021, **13**, 53.
3 X. Hou, C. Ke, C. J. Bruns, P. R. McGonigal, R. B. Pettman and J. F. Stoddart, *Nat. Commun.*, 2015, **6**, 6884.
4 H. Wang, X. Ji, Z. A. Page and J. L. Sessler, *Mater. Chem. Front.*, 2020, **4**, 1024–1039.
5 Y. Wang, X. Tan, Y.-M. Zhang, S. Zhu, I. Zhang, B. Yu, K. Wang, B. Yang, M. Li, B. Zou and S. X.-A. Zhang, *J. Am. Chem. Soc.*, 2015, **137**, 931–939.
6 Z. Peng, X. Feng, B. Tong, D. Chen, J. Shi, J. Zhi and Y. Dong, *Sens. Actuators, B*, 2016, **232**, 264–268.
7 K. Li, T.-B. Ren, S. Huan, L. Yuan and X.-B. Zhang, *J. Am. Chem. Soc.*, 2021, **143**, 21143–21160.
8 D. Su, C. L. Teoh, L. Wang, X. Liu and Y.-T. Chang, *Chem. Soc. Rev.*, 2017, **46**, 4833–4844.
9 F. Gao, R. Du, C. Han, J. Zhang, Y. Wei, G. Lu and H. Xu, *Chem. Sci.*, 2019, **10**, 5556–5567.
10 X. Huang, L. Qian, Y. Zhou, M. Liu, Y. Cheng and H. Wu, *J. Mater. Chem. C*, 2018, **6**, 5075–5096.
11 W. Z. Yuan, Y. Tan, Y. Gong, P. Lu, J. W. Y. Lam, X. Y. Shen, C. Feng, H. H.-Y. Sung, Y. Lu, I. D. Williams, J. Z. Sun, Y. Zhang and B. Z. Tang, *Adv. Mater.*, 2013, **25**, 2837–2843.
12 P. S. Hariharan, D. Moon and S. P. Anthony, *J. Mater. Chem. C*, 2015, **3**, 8381–8388.
13 R. Li, S. Xiao, Y. Li, Q. Lin, R. Zhang, J. Zhao, C. Yang, K. Zou, D. Li and T. Yi, *Chem. Sci.*, 2014, **5**, 3922–3928.
14 Y. Hong, J. W. Y. Lam and B. Z. Tang, *Chem. Soc. Rev.*, 2011, **40**, 5361–5388.
15 J. Luo, Z. Xie, J. W. Y. Lam, L. Cheng, H. Chen, C. Qiu, H. S. Kwok, X. Zhan, Y. Liu, D. Zhu and B. Z. Tang, *Chem. Commun.*, 2001, 1740–1741.
16 W. Z. Yuan, P. Lu, S. Chen, J. W. Y. Lam, Z. Wang, Y. Liu, H. S. Kwok, Y. Ma and B. Z. Tang, *Adv. Mater.*, 2010, **22**, 2159–2163.
17 Z. Zhao, H. Zhang, J. W. Y. Lam and B. Z. Tang, *Angew. Chem., Int. Ed.*, 2020, **59**, 9888–9907.
18 J. Mei, Y. Hong, J. W. Y. Lam, A. Qin, Y. Tang and B. Z. Tang, *Adv. Mater.*, 2014, **26**, 5429–5479.
19 K. Wang, H. Zhang, S. Chen, G. Yang, J. Zhang, W. Tian, Z. Su and Y. Wang, *Adv. Mater.*, 2014, **26**, 6168–6173.
20 B. Zhang, J. Jiang, W. Wang, Q. Tu, R. Yu, J. Wang and M.-S. Yuan, *Mater. Chem. Front.*, 2022, **6**, 613–622.
21 J. N. Zhang, H. Kang, N. Li, S. M. Zhou, H. M. Sun, S. W. Yin, N. Zhao and B. Z. Tang, *Chem. Sci.*, 2017, **8**, 577–582.
22 P. S. Hariharan, G. Parthasarathy, A. Kundu, S. Karthikeyan, Y. Sagara, D. Moon and S. P. Anthony, *Cryst. Growth Des.*, 2018, **18**, 3971–3979.
23 W. Zhao, Z. He, Q. Peng, J. W. Y. Lam, H. Ma, Z. Qiu, Y. Chen, Z. Zhao, Z. Shuai, Y. Dong and B. Z. Tang, *Nat. Commun.*, 2018, **9**, 3044.
24 Q. Luo, C. Lv, H. Sheng, F. Cao, J. Sun, C. Zhang, M. Ouyang, B. Zou and Y. Zhang, *Adv. Opt. Mater.*, 2020, **8**, 1901836.
25 S. Guo, G. Zhang, L. Kong, Y. Tian and J. Yang, *Chem. – Eur. J.*, 2020, **26**, 3834–3842.
26 J. Zhao, Z. Chi, Y. Zhang, Z. Mao, Z. Yang, E. Ubba and Z. Chi, *J. Mater. Chem. C*, 2018, **6**, 6327–6353.
27 Y. Chen, B. Wang, Y. Lei, Y. Zhou, Y. Guo, M. Liu, W. Gao, X. Huang and H. Wu, *Mater. Chem. Front.*, 2022, **6**, 459–465.
28 P. S. Hariharan, C. Pan, S. Karthikeyan, D. Xie, A. Shinohara, C. Yang, L. Wang and S. P. Anthony, *Dyes Pigm.*, 2020, **174**, 108067.
29 C. Ge, J. Liu, X. Ye, Q. Han, L. Zhang, S. Cui, Q. Guo, G. Liu, Y. Liu and X. Tao, *J. Phys. Chem. C*, 2018, **122**, 15744–15752.
30 Y. Liu, A. Li, S. Xu, W. Xu, Y. Liu, W. Tian and B. Xu, *Angew. Chem., Int. Ed.*, 2020, **59**, 15098–15103.
31 M. Fourmigué and P. Batail, *Chem. Rev.*, 2004, **104**, 5379–5418.
32 P. Metrangolo, F. Meyer, T. Pilati, G. Resnati and G. Terraneo, *Angew. Chem., Int. Ed.*, 2008, **47**, 6114–6127.
33 E. Persch, O. Dumele and F. Diederich, *Angew. Chem., Int. Ed.*, 2015, **54**, 3290–3327.
34 P. Rajamalli, P. Gandeepan, M.-J. Huang and C.-H. Cheng, *J. Mater. Chem. C*, 2015, **3**, 3329–3335.
35 C. Ma, X. Zhang, Y. Yang, Z. Ma, L. Yang, Y. Wu, H. Liu, X. Jia and Y. Wei, *Dyes Pigm.*, 2016, **129**, 141–148.
36 Y. Qi, Y. Wang, Y. Yu, Z. Liu, Y. Zhang, G. Du and Y. Qi, *RSC Adv.*, 2016, **6**, 33755–33762.
37 A. D'Aléo, A. Saul, C. Attaccalite and F. Fages, *Mater. Chem. Front.*, 2019, **3**, 86–92.
38 Z. Zhou, Q. Liu, X. Chen, G. Xu, S. Wang, Y. Tu, J. Zhang, X. Zheng, J. Xiang, X. Feng, Y. Zhang, S. Xie, Z. Zeng and B. Z. Tang, *Adv. Funct. Mater.*, 2021, **31**, 2009024.
39 Y. Chen, Y. Zhou, Z. Wang, M. Wang, W. Gao, Y. Zhou, M. Liu, X. Huang and H. Wu, *CrystEngComm*, 2019, **21**, 4258–4266.
40 H. Li, H. Shu, Y. Liu, X. Wu, H. Tian, H. Tong and L. Wang, *Adv. Opt. Mater.*, 2019, **7**, 1801719.
41 P. Xue, B. Yao, J. Sun, Q. Xu, P. Chen, Z. Zhang and R. Lu, *J. Mater. Chem. C*, 2014, **2**, 3942–3950.
42 P. Gayathri, S. Karthikeyan, M. Pannipara, A. G. Al-Sehemi, D. Moon and S. P. Anthony, *CrystEngComm*, 2019, **21**, 6604–6612.
43 J. Wang, X. Gu, H. Ma, Q. Peng, X. Huang, X. Zheng, S. H. P. Sung, G. Shan, J. W. Y. Lam, Z. Shuai and B. Z. Tang, *Nat. Commun.*, 2018, **9**, 2963.
44 K. Kanosue and S. Ando, *ACS Macro Lett.*, 2016, **5**, 1301–1305.

45 A. Forni, E. Lucenti, C. Botta and E. Cariati, *J. Mater. Chem. C*, 2018, **6**, 4603–4626.
46 S. Gan, S. Hu, X.-L. Li, J. Zeng, D. Zhang, T. Huang, W. Luo, Z. Zhao, L. Duan, S.-J. Su and B. Z. Tang, *ACS Appl. Mater. Interfaces*, 2018, **10**, 17327–17334.
47 H. Shi, Z. An, P.-Z. Li, J. Yin, G. Xing, T. He, H. Chen, J. Wang, H. Sun, W. Huang and Y. Zhao, *Cryst. Growth Des.*, 2016, **16**, 808–813.
48 W. A. Morris, T. Liu and C. L. Fraser, *J. Mater. Chem. C*, 2015, **3**, 352–363.
49 A. Ghodbane, N. Saffon, S. Blanc and S. Fery-Forgues, *Dyes Pigm.*, 2015, **113**, 219–226.
50 J. Zhou, L. Liu, Y. Pan, Q. Zhu, Y. Lu, J. Wei, K. Luo, Y. Fu, C. Zhong, Y. Peng and Z. Song, *Chem. – Eur. J.*, 2018, **24**, 17897–17901.
51 M. Qayyum, T. Bushra, Z. A. Khan, H. Gul, S. Majeed, C. Yu, U. Farooq, A. J. Shaikh and S. A. Shahzad, *ACS Omega*, 2021, **6**, 25447–25460.
52 L. Wang, R. Zhang, Z. Huang, S. Guo, J.-X. Yang and L. Kong, *Dyes Pigm.*, 2022, **197**, 109909.
53 C. Wang and Z. Li, *Mater. Chem. Front.*, 2017, **1**, 2174–2194.
54 Z. Yang, Z. Chi, Z. Mao, Y. Zhang, S. Liu, J. Zhao, M. P. Aldred and Z. Chi, *Mater. Chem. Front.*, 2018, **2**, 861–890.
55 Y. Yin, Z. Chen, C. Fan, G. Liu and S. Pu, *ACS Omega*, 2019, **4**, 14324–14332.
56 Z. Qiu, Z. Yang, W.-C. Chen, L. Xing, S. Hu, S. Ji, Q. Yang, N. Cai, X. Ouyang and Y. Huo, *J. Mater. Chem. C*, 2020, **8**, 4139–4147.
57 J. Shi, N. Chang, C. Li, J. Mei, C. Deng, X. Luo, Z. Liu, Z. Bo, Y. Q. Dong and B. Z. Tang, *Chem. Commun.*, 2012, **48**, 10675–10677.
58 Z. Zhang, Z. Wu, J. Sun, B. Yao, P. Xue and R. Lu, *J. Mater. Chem. C*, 2016, **4**, 2854–2861.
59 S. Zhang, Y. Huang, L. Kong, X. Zhang and J. Yang, *Dyes Pigm.*, 2020, **181**, 108574.